UCRL-JRNL-229316

Compulsory Deep Mixing of 3He and CNO Isotopes in the Envelopes of low-mass Red Giants

P. P. Eggleton, D. S. P. Dearborn, J. C. Lattanzio

March 22, 2007

Astrophysical Journal

Disclaimer

Not to appear in Nonlearned J., 45.

Compulsory Deep Mixing of ^{3}He and CNO Isotopes in the Envelopes of low-mass Red Giants

Peter P. Eggleton[1], David S. P. Dearborn[1] and John C. Lattanzio[2]

[1]*Lawrence Livermore National Laboratory, 7000 East Ave, Livermore, CA94551, USA*

[2]*Monash University, Mathematics Department, Clayton, Victoria, 3168, Australia*

ppe@igpp.ucllnl.org, dearborn2@llnl.gov, john.lattanzio@sci.monash.edu.au

ABSTRACT

Three-dimensional stellar modeling has enabled us to identify a deep-mixing mechanism that must operate in all low mass giants. This mixing process is not optional, and is driven by a molecular weight inversion created by the ^{3}He(^{3}He,2p)^{4}He reaction. In this paper we characterize the behavior of this mixing, and study its impact on the envelope abundances. It not only eliminates the problem of ^{3}He overproduction, reconciling stellar and big bang nucleosynthesis with observations, but solves the discrepancy between observed and calculated CNO isotope ratios in low mass giants, a problem of more than 3 decades' standing. This mixing mechanism operates rapidly once the hydrogen burning shell approaches the material homogenized by the surface convection zone. In agreement with observations, Pop I stars between 0.8 and 2.0 $M_\odot$ develop ^{12}C/^{13}C ratios of 14.5 $\pm$ 1.5, while Pop II stars process the carbon to ratios of 4.0 $\pm$ 0.5. In stars less than 1.25 $M_\odot$, this mechanism also destroys 90% to 95% of the ^{3}He produced on the main sequence.

Subject headings: stars: red giants; abundance anomalies

1. Introduction

In a previous paper (Dearborn et al. 2006; hereinafter Paper I) we used a fully 3-dimensional code `Djehuty`, developed in the Lawrence Livermore National Laboratory, to investigate the onset of the helium flash in a low-mass red giant. While convective motion

due to the helium flash was seen to occur in much the same region as predicted by one-dimensional (spherically symmetric) models, we noticed some minor motion, apparently also of a turbulent convective character, in an unexpected region: a region above but not far above the hydrogen-burning shell, and well below the base of the conventional surface convection zone. This is visible in Fig. 14 of Paper I. On subsequent close inspection we found that this additional motion was due to a very small molecular-weight inversion, which was Rayleigh-Taylor unstable. This inversion in turn was due to the burning of ^{3}He, of which quite a high concentration is left by the retreating surface convection zone.

In two futher papers (Eggleton et al. 2006a,b; hereinafter Papers II, III) we showed why such an inversion is expected to arise, once the surface convection zone, having reached its deepest extent, begins to retreat. Furthermore, we suggested that this motion should grow in extent so that it reaches from the base of the normal surface convection zone downwards to the point where ^{3}He is able to burn. It should lead to the destruction of most ($>90\%$) of the ^{3}He in the surface layers, and it should simultaneously allow for some processing of ^{12}C to ^{13}C. Thus at the surface of the star ^{3}He should be progressively depleted, and ^{13}C progressively enhanced, beyond the values expected from conventional 1D models.

In this paper we consider further the effect of our additional mixing, which we refer to as 'μ-boosted mixing'. We would like to emphasise that this mixing can explain in a natural way observed abundances that have hitherto been attributed to *ad hoc* mechanisms like rotation and magnetic fields. We would also like to emphasise the value of 3D modeling. It was only by using a fully 3D model that this mixing was noticed. It is due to a very slight effect, a μ-inversion that amounts to only about one part in 10^4, and yet it is quite obvious in a 3D simulation. One can in fact see the inversion in 1D models – although we are not aware that anyone has actually commented on it – but in 1D models mixing only sets in if the code-developer tells the code to include it.

3D simulations are expensive of computer time. Our philosophy in using `Djehuty` has been that 3D simulations spanning a short period of time may allow us insight into complex hydrodynamic and hydromagnetic phenomena which will then enable us to improve the quality of simplistic 1D models. We follow this principle here. We introduce into our 1D code a convective mixing coefficient that depends on the μ-gradient, but only if the μ-gradient is in the sense that it is destabilising. This is in addition to the mixing coefficient that is due to ordinary convective instability, which depends (crudely speaking) on the entropy gradient but also only if this gradient has the sign which is destabilising.

In Section 2 we discuss the significance of possible mixing for abundance measurements on the Giant Branch. In Section 3 we discuss our new μ-boosted mixing mechanism in more detail. In Section 4 we describe a 1D code which incorporates a simple model of our

μ-boosted mixing. In Sections 5 and 6 we discuss the sensitivity of this model to some input parameters that we estimate. In Sections 7 – 12 we present our results and conclusions.

2. The Importance of Mixing on the Giant Branch

There is a long history of observing the carbon, nitrogen and oxygen (CNO) isotope ratios in Red Giants (Lambert & Dearborn 1972, Day et al. 1974, Dearborn et al. 1975, 1976, Tomkin et al. 1975, 1976, Tomkin & Lambert 1978, Harris & Lambert 1984a,b, Gilroy 1989) as a probe of stellar interiors and evolution. While on the main sequence, nuclear reactions change the abundance distribution in a star's deep envelope. These changes are then mixed to the surface when the star becomes a giant. Among the isotopes that are substantially enhanced by low mass stars are ^{3}He, ^{13}C and ^{17}O. Other isotopes like ^{15}N and ^{18}O are reduced. Distressingly, these ratios were nearly always different from what was expected, and sometimes very different (Dearborn et al. 1976, Dearborn 1992).

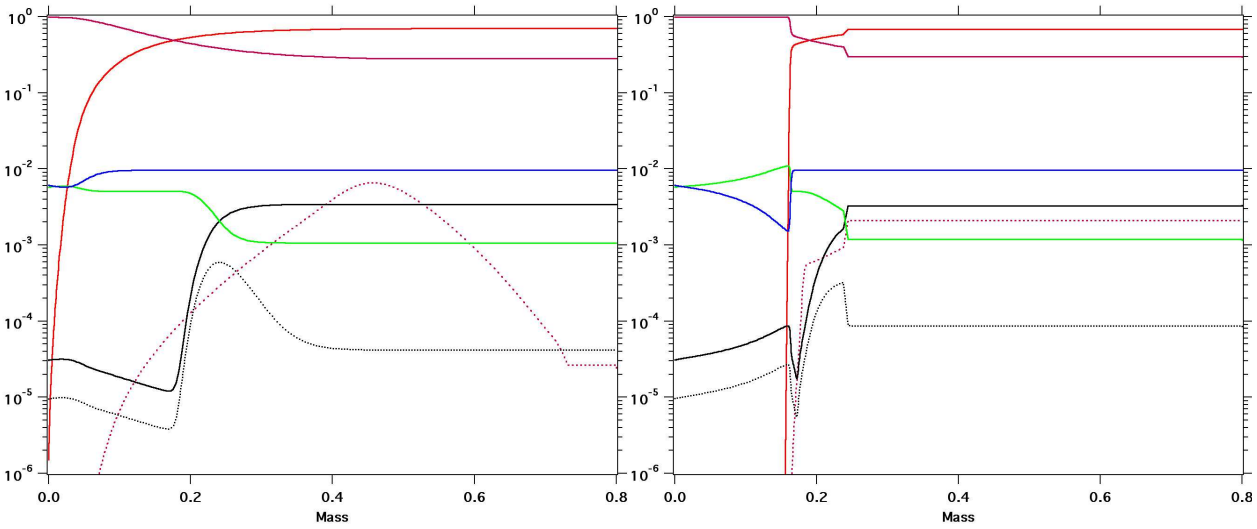

Figure 1 – Composition structure of a 0.85 $M_{\odot}$ Pop I model (left) near the end of its main-sequence life, and (right) near the deepest penetration of the surface convective region on the giant branch. ^{1}H – vermilion; ^{4}He – magenta; ^{12}C – black; ^{16}O – blue; ^{12}C – green; ^{3}He – red dots; ^{13}C – black dots.

A result of giant-branch abundance changes that is of particular consequence is the robust result that low mass stars (below $\sim$1.5 $M_{\odot}$) are major producers of ^{3}He. In these stars, the PP chain produces a ^{3}He-rich peak in the envelope of the star. Giant-branch convection homogenizes this region, raising the surface ^{3}He abundance by a factor of $\sim$80

(see Fig. 1). As the helium core grows some ^{3}He is destroyed; however, in classical 1D models, the fractional abundance of ^{3}He in the convective envelope is not diminished, even although the extent of the envelope (in terms of mass fraction) is diminished. The presence of horizontal branches in the HR diagrams of globular clusters can be understood only if substantial amounts of envelope mass are lost on the giant branch. This should result in a substantial enhancement of the ^{3}He in the interstellar medium, by low mass stars of both Pop I and Pop II (Dearborn et al. 1986, Steigman et al. 1986, Dearborn et al. 1996). Work by Hata et al. (1995) argued that unless $>90\%$ of this ^{3}He is destroyed prior to ejection, the results of stellar nucleosynthesis come into conflict with standard Big Bang Nucleosynthesis. To avoid this, there must be some mechanism that operates well before the helium core flash to destroy the ^{3}He.

Smith & Tout (1992) and Wasserburg et al. (1995) posited that a deep circulation mechanism could solve the problem of low ^{12}C/^{13}C values observed in red giants, and destroy the excess ^{3}He at the same time. Mechanisms have been explored that might cause anomalous deep mixing, including magnetic-field generation (Hubbard & Dearborn 1980) or rotational mixing (Charbonnel 1995, Chaname et al. 2005, Palacios et al. 2006). The necessity for some deep mixing was also discussed by Hogan (1995).

To destroy the necessary ^{3}He, any such mechanism must operate efficiently in nearly all low mass stars. While rotation is certainly present in young stars it is observed to decay on the main sequence. The slow rotation speeds seen in white dwarfs, and the rotation rate inferred in the Solar core by helioseismology, suggest that angular momentum is not conserved in the cores either. As a consequence, dependence on the ability of rotation to destroy the excess ^{3}He in all long-lived stars is unsettling. Nevertheless, rotational mixing must surely exist as an added mechanism in some stars.

Here, we wish to extend the results obtained on a new mixing mechanism, described by Eggleton et al. (2006a, b; henceforth Papers II and III), that operates efficiently in all low mass stars. This new mechanism is not optional: it inevitably arises on the First Giant Branch when the hydrogen-burning shell encroaches on the homogenised, formerly convective, zone left behind by the retreating convective envelope, and begins to burn ^{3}He. The ^{3}He burning occurs just outside the normal hydrogen-burning shell, at the base of a radiatively stable region about $1\,R_\odot$ in thickness. The burning causes a molecular weight inversion, which creates a Rayleigh-Taylor instability that drives mixing all the way to the usual convection zone. As we will show, it not only routinely destroys $>90\%$ of the ^{3}He produced in the low-mass offenders, but reduces the ^{12}C/^{13}C ratios from the range of 20 to 35 down to the observed values between 5 and 15, depending on metallicity..

3. The μ-Boost Mechanism

As described above, this mixing mechanism is activated when the hydrogen-burning shell approaches the homogenized region left behind by the retreating surface convection zone. ^{3}He is among the most fragile nuclei present, and the reaction

$$^3\mathrm{He}\ (^3\mathrm{He},2\mathrm{p})\ ^4\mathrm{He}\ , \tag{1}$$

has the unusual characteristic (among reactions in stars) of lowering the mean molecular weight μ, creating a localised μ-inversion. This inversion is only about $0.025\,R_\odot$ above the helium ($X = 0$) core, and has the lowest molecular weight in the entire star (Fig. 2).

We emphasise that the ^{3}He-burning at this stage produces an inversion only because of the previous homogenisation of the outer layers by the surface convection. Substantial ^{3}He is produced early in the star's life (i.e. on the main sequence) and would certainly be burnt later when the hydrogen-burning shell has moved out far enough. But there would be no μ-inversion, because the ^{3}He peak would be superimposed on a ^{1}H/^{4}He gradient that gives a strongly stabilising μ-gradient. However when the entire outer layers are homogenised by convection, and then later gradually released towards the burning shell, the background gradient has been removed and so the inversion can stand out (even though it is very small; see Fig. 2).

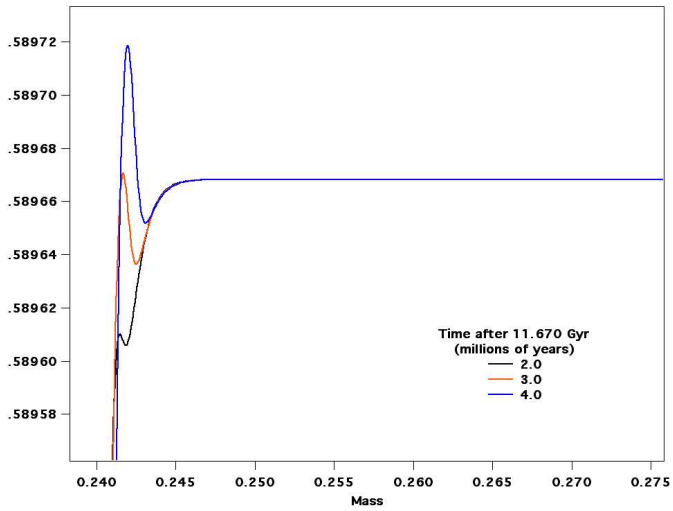

Figure 2 – The development of a molecular-weight inversion is shown (versus mass) for a $1.0\,M_\odot$ Pop I model. $1/\mu$ curves are shown for million-year increments beginning at 11.67 Gyr.

As shown in Paper II, such an inversion leads to rapidly rising clouds of hydrogen-enhanced, ^{3}He-depleted material. A simple buoyancy argument was used to estimate the rise

rate of these clouds to be of order 100 m/s, only modestly slower than the speeds expected in the convection region itself, and our three-dimensional modeling of a $1\,M_\odot$ ($Z = 0.02$) star using the LLNL code `Djehuty` (Papers I, II) did indeed show such speeds. As these clouds rise (Fig. 3), they are replaced with ^{3}He-rich material, and the process is continued. If such speeds are maintained, the low-molecular-weight material will reach the convection zone in a few months. This is to be compared to the hundreds of millions of years required for a low mass star to reach the helium flash after this μ-boosted process begins.

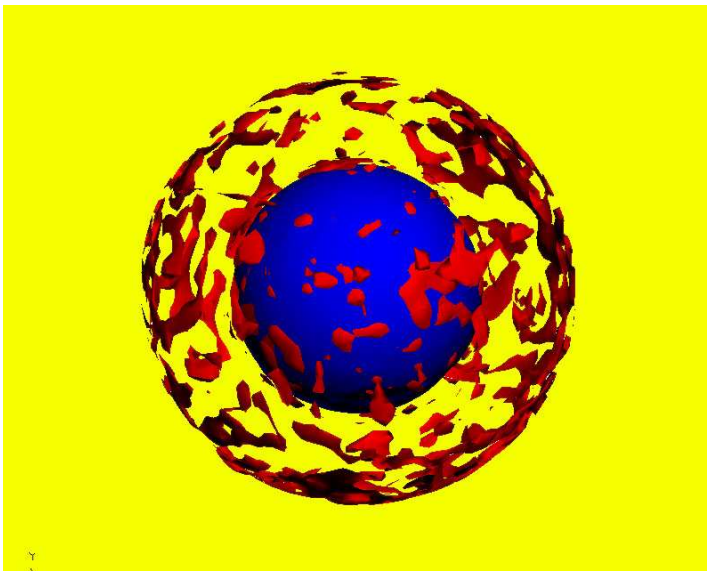

Figure 3 – the location of the hydrogen burning shell is shown by a blue contour at a fixed mass fraction of ^{14}N. Shown in red are rising clouds in which the hydrogen abundance is marginally higher than in the surrounding material.

The disparity of the mixing to evolutionary timescale is such that Paper III used an instantaneous mixing approximation and the temperature/density structure of the stable region to estimate the amount of ^{3}He-processing. In the time taken by a $1\,M_\odot$ star to evolve up the giant branch, the ^{3}He in the envelope was expected to decline by about 3 e-folds or 95%. A similar estimate for ^{12}C-processing indicated that ^{12}C would decrease by about 8%. While modest, this is sufficient to reduce the ^{12}C/^{13}C ratio from 25 to near 15.

This analytic calculation suggested that the μ-boosted mixing might solve more than the conflict between the Big Bang nucleosynthesis and stellar evolution as to which produced the ^{3}He. It has the potential to solve many of the CNO isotope anomalies. Weiss & Charbonnel (2004) have identified the point where CNO composition differences (from expected values) begin to occur as 'where the hydrogen-burning shell encounters the deepest point to which the convective envelope ever reached', and this is just where the μ-boost mechanism becomes

operational.

To examine this possibility quantitatively, we have incorporated a μ-boosted mixing model into a 1D stellar evolution code. The code tracks 16 isotopes, including all stable isotopes of the CNO tri-cycle: ^{1}H, ^{2}H, ^{3}He, ^{4}He, ^{12}C, ^{13}C, ^{14}N, ^{15}N, ^{16}O, ^{17}O, ^{18}O, ^{20}Ne, ^{21}Ne, ^{22}Ne, ^{23}Na, ^{1}n. They are coupled through reaction rates taken from Caughlan & Fowler (1988). Following their recommendation, in reactions like ^{17}O(p,α)^{14}N and ^{17}O(p,γ)^{18}F that have an uncertain factor (0 to 1) on certain states, the factor was chosen to be 0.1. As discussed by Dearborn (1992), these factors are significant for the expected oxygen isotope ratios. In the sections below, this model will be tested and used to explore a range of masses and metallicities.

4. The Speed of μ-Boosted Mixing

In the absence of μ-boosted mixing, the magnitude of the inversion depends on the ^{3}He abundance. The temperature in the region where ^{3}He is burned is $\gtrsim 10^{7}$K, so that the material is fully ionised. The mean molecular weight is

$$\frac{1}{\mu} = \sum_i \frac{(Z_1+1)X_i}{A_i} \ . \tag{2}$$

The ^{3}He cross-section is larger than other rates, resulting in the production of ^{4}He and ^{1}H and reducing the molecular weight. Through reaction (1) μ decreases by an amount that depends on the change in the ^{3}He mass fraction:

$$\frac{\delta\mu}{\mu^2} \ = \ \frac{\delta X_3}{6} \ < \ 0 \ . \tag{3}$$

The nuclear reaction is exothermic, and the daughter particles are produced with energies substantially above the temperature of the surrounding medium. However for present purposes let us ignore this and consider only the effect of the molecular weight change, holding the temperature to be the same. For an ideal gas the mean μ change ($\delta\mu < 0$) increases the pressure:

$$\frac{\delta P}{P} \ = \ -\frac{\delta\mu}{\mu} = -\frac{\mu\delta X_3}{6} \ . \tag{4}$$

To maintain hydrostatic equilibrium the gas expands, the density drops, and the element of fluid becomes buoyant. We (Paper II) used an energy argument to estimate that the element rises at a speed

$$v \ \sim \ \left(g h_{\rm P} \frac{|\delta\mu|}{\mu} \right)^{1/2} \ \sim \ 200\,{\rm m/s} \ , \tag{5}$$

g being the local gravity and $h_{\rm P}$ the local pressure scale height. This estimate is about half that expected near the base of the normal surface convection zone. Initial speeds of this magnitude were confirmed through 3D modeling with the LLNL code `Djehuty`. As it rises, the density drops in both the bubble and the surrounding environment. Assuming no enhancement in temperature from the ^{3}He burning, the initial density deficit in the bubble (compared to its surroundings) is

$$\left(\frac{\delta\rho}{\rho}\right)_{\rm init} \;=\; \frac{\mu\delta X_3}{6} \;. \tag{6}$$

Because the surroundings are stable against normal convection, the density outside the bubble will drop at a rate that differs from that in the bubble itself. The bubble will cease being buoyant after some distance δr when the density and pressure of the bubble both equal those of the surroundings:

$$\delta\rho_{\rm init} = \delta\rho_{\rm rad} - \delta\rho_{\rm ad} \;=\; -\,\rho(\nabla_{\rm rad} - \nabla_{\rm ad})\,\frac{d\ln P}{dr}\,\delta r \;, \tag{7}$$

so that

$$\delta r \approx \frac{h_{\rm P}\,\mu\,|\delta X_3|}{6(\nabla_{\rm rad} - \nabla_{\rm ad})} \;. \tag{8}$$

Evaluating this for a $1\,M_\odot$ Pop I star just after the inversion starts, we find that the bubbles will rise all the way to the normal convection zone ($\Delta r \sim 3\times10^5\,$km) *if* the envelope were pure ^{3}He. But the mass fraction is only $\sim10^{-3}$, and so the bubbles could rise for $\sim 3\times10^2$km before coming into density and pressure equilibrium with the surroundings.

Our `Djehuty` calculation began from an artificial situation, in that the μ-inversion had been allowed to grow to its maximum size already in the previous 1D calculation. We therefore see rather rapid motion setting in rather quickly. In practice, the motion should have started as soon as the inversion began, and the motion set up by that, though slower, would have prevented the inversion building up to the size that we see in Fig. 2. We attempt to make a realistic estimate of the slower motion that we would expect to be set up in a roughly steady state.

In a real stellar environment the buoyancy will begin when only a fraction of the ^{3}He is processed, and it will move only a short distance before coming to hydrostatic equilibrium. When the bubble reaches this new equilibrium, its temperature will be lower than its surroundings by an amount

$$\frac{\delta T}{T} \;=\; \frac{\delta\mu}{\mu} \;. \tag{9}$$

Heat will diffuse in, and the bubble will continue to rise on a thermal timescale. As a crude estimate we can take the mixing time to be of the same order as the thermal timescale,

defined as the thermal energy in the radiative layer divided by the luminosity, i.e. about $\tau \sim 5000\,\mathrm{yrs}$. This gives an estimate (probably a considerable underestimate) of the mixing speed:

$$v \;>\; \frac{\Delta r}{\tau} \sim 0.2\,\mathrm{cm/s}\ . \tag{10}$$

We attempt to make a somewhat sharper estimate of the speed with which the bubble will rise. Consider a bubble of radius l with lower-μ material. The rate with which heat energy enters the bubble can be estimated as

$$F \sim 4\pi l^2\,.\,acT^3\delta T \sim 4\pi l^2 acT^4 \frac{|\delta\mu|}{\mu}\ . \tag{11}$$

As flux enters the low-temperature region, the temperature increases at a rate that depends on the volume:

$$F \sim \frac{4}{3}\,\pi\,l^3\,\frac{3}{2}\frac{\rho N_0 k}{\mu}\,\frac{dT}{dt}\ , \tag{12}$$

and so

$$\frac{dT}{dt} \sim \frac{2acT^4}{\rho N_0 k l}\,|\delta\mu|\ . \tag{13}$$

The temperature gradient that must be overcome is

$$\frac{dT}{dr} \;=\; \frac{T}{P}\,\nabla_{\mathrm{rad}}\,g\rho\ . \tag{14}$$

This is accomplished as energy flows into the bubble resulting in a rise velocity of

$$v \;\sim\; \frac{dT/dt}{dT/dr} \;\sim\; \frac{2acT^4}{gl\rho\nabla_{\mathrm{rad}}}\,\frac{|\delta\mu|}{\mu}\ . \tag{15}$$

The factor $|\delta\mu|/\mu$ is set at the deepest level of the mixing region where the heat from the H-burning shell drives the ^{3}He reaction. This gives

$$\frac{|\delta\mu|}{\mu} \;=\; -\,\frac{\mu\delta X_3}{6} \;=\; \frac{l\mu}{6v}\,\frac{dX_3}{dt} \;=\; \frac{1}{2}N_0\rho\left(\frac{X_3}{3}\right)^2 R_{\mathrm{nuc}}\,\frac{l\mu}{6v}\ , \tag{16}$$

where R_{nuc} is the thermal average of reaction cross-section times speed. Then combining (15) and (16),

$$v^2 \;=\; \frac{acT^4 N_0 R_{\mathrm{nuc}}\mu}{6g\nabla_{\mathrm{rad}}}\left(\frac{X_3}{3}\right)^2\ . \tag{17}$$

Evaluating these terms in the region where ^{3}He is burned, for a $1\,M_\odot$ Pop I star, gives a rising speed in the bubble of $\sim 2\,\mathrm{cm/s}$. This is a good deal smaller than the estimate (5), but an order of magnitude above the crude estimate (10), and is limited by the burning rate of

^{3}He. It applies only while the bubble of low μ is establishing itself, during which the μ-deficit reaches

$$\frac{|\delta\mu|}{\mu} \sim 5 \times 10^{-9} \ . \tag{18}$$

Once $|\delta\mu|/\mu$ is established, it can be held constant and equation (15) used to calculate the speed. This speed will be typically somewhat larger than the initial speed.

Averaged over the classically stable region, equation (15) in Pop I models show speeds of $\sim 1 - 2\,\mathrm{m/s}$. Pop II models develop lower $|\delta\mu|/\mu$ values, and average velocities nearer $0.5\,\mathrm{m/s}$. This estimate was repeated for several core masses as the model evolved up the FGB, resulting in mixing times of between 10 and 50 years. Models of different mass were also examined, with the result that lower-mass models mix somewhat more slowly and higher-mass models somewhat faster. Still, for Pop I models the mixing timescale was under 100 years (Fig. 4).

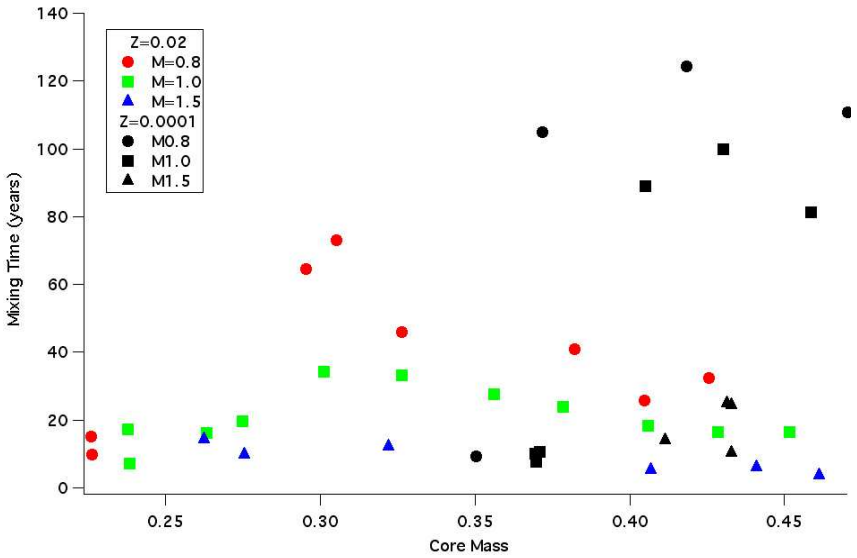

Figure 4 – Mixing times along the giant branch, for Pop I and Pop II models with a range of masses.

Extreme Pop II models ($Z = 0.0001$) were also examined. The initial mixing in these models starts at higher temperatures, resulting in greater values of $|\delta\mu|/\mu$. The mixing timescales start near 10 years for all the masses examined. However, as these models evolved the timescal rapidly increased to ~ 100 years. This is probably a result of the rapid destruction of ^{3}He. A mixing time of 100 years is about 0.01% of the time to burn through the

classically stable region. We can argue that the classically stable region will be homogenised with the classically convective surface zone on a short timescale.

The process of thermally-driven buoyancy described by equation (15) should leave the temperature gradient radiative, but leads to elongated vertical structures resembling 'salt-fingers' (Wilson & Mayle 1988, Dalhed et al. 1999). As energy diffuses into the outer portion of the bubbles, the material rises, exposing the inner material. These slender structures have more surface area per unit volume than the bubble model used here, allowing energy to diffuse more rapidly into the low-μ material, and this results in higher rise velocities than our estimate here.

5. The μ-Boosted Mixing Model

In 1D codes, mixing always requires some physical model to approximate the process. Our 1D code treats convection as a diffusion process and solves a second-order equation for each isotope:

$$\left(\frac{\partial X}{\partial t}\right)_k = \frac{\partial}{\partial m}\sigma\frac{\partial X}{\partial m} + R + \frac{\partial X}{\partial m}\left(\frac{\partial m}{\partial t}\right)_k \ . \tag{19}$$

The first term in the equation for the rate of change of the isotope is for the convective diffusion, the next term (R) incorporates the nuclear reaction rates, and there is a final term to deal with the mesh motion, because the mesh is non-Lagrangian.

In a standard convective region the diffusion coefficient σ that we use takes a form that scales quadratically with the temperature-gradient excess over the adiabatic value, and inversely with the nuclear timescale:

$$\sigma = \frac{F_{\rm conv}}{t_{\rm nuclear}}\left(r\,\frac{\partial m}{\partial r}\right)^2 \left[\max(0, \nabla_r - \nabla_a)\right]^2 \ , \tag{20}$$

where ∇_r and ∇_a are the usual radiative and adiabatic temperature gradients from the mixing-length theory of convection. The dimensionless and largely arbitrary factor $F_{\rm conv}$ is simply chosen to be a large number such that the composition in a convective region homogenizes in a time much shorter than the nuclear time scale ($t_{\rm nuclear}$). To model our μ-boosted process we have created a diffusion coefficient wherever there is an inversion. The form that we have used is:

$$\begin{aligned}\sigma &= \frac{F_{\rm inv}}{t_{\rm nuclear}}\left(r\,\frac{\partial m}{\partial r}\right)^2 (\mu - \mu_{\rm min}) \quad (k > k_{\rm min}) \\ &= 0 \quad (k \le k_{\rm min}) \ ,\end{aligned} \tag{21}$$

where (a) $\mu_{\rm min}$ is the smallest value of μ in the current model, (b) $\mu_{\rm min}$ occurs at meshpoint number $k_{\rm min}$, and (c) k, the meshpoint number, is counted outwards from the center. Again, the factor $F_{\rm inv}$, if large, simply assures homogeneity in a time much shorter than the nuclear time scale. To estimate the speed that corresponds to a chosen factor value, we performed a numerical test in which a step function was installed in an element that was not being used in the nucleosynthesis network. The position of the step was located just above the point where the inversion would form. Below this point, the mass fraction was set to 10^{-7}, and above this point dropped to 10^{-10}. Once the inversion develops, mixing begins, and a stable gradient is formed. The rate at which the material below the step is transported to the surface was then monitored to obtain an effective speed (with the usual convective diffusion coefficient turned off to avoid confusion). This is illustrated in Fig. 5.

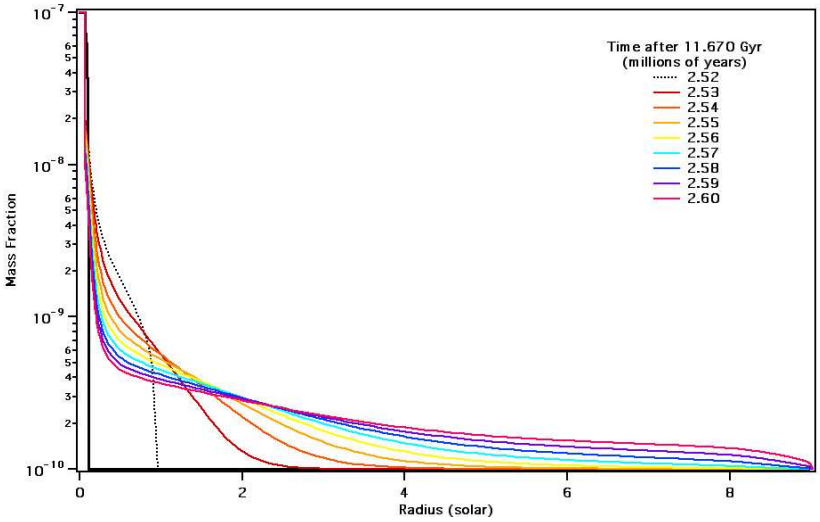

Figure 5 – The mass fraction profile created by the proposed diffusion coefficient in a $1\,M_\odot$ star ($Z = 0.02$), starting from a pure step-function profile. Each curve is separated by 10,000 years. For the value of $F_{\rm inv}$ selected here, the speed at which the material is carried outward corresponds to about 0.3 cm/s.

Various values of $F_{\rm inv}$ were tested in a $1\,M_\odot$ Pop I model, and a value selected to be the standard. For this value, the speed with which the composition rise moved outward in the star averaged about 0.3 cm/s. Increasing $F_{\rm inv}$ by 10 times results in a speed that approached 1.5 cm/s. Increasing this arbitrary value by another factor of 10 (100 times the standard value) again increases the speed to 6 cm/s. All of these speeds are much less that expected from the previous work (Papers II, III). Nevertheless they are sufficient to mix the stable region with the outer convective region on a time that is short in comparison to the evolution. These speeds are near the startup velocity found where the reduced $|\delta\mu|/\mu$ is

established, where the nucleosynthesis is done, and where the composition changes are most sensitive to mixing speed. The effective transport speeds are a bit less than expected for a steady salt-finger like growth through the bulk of the stable region.

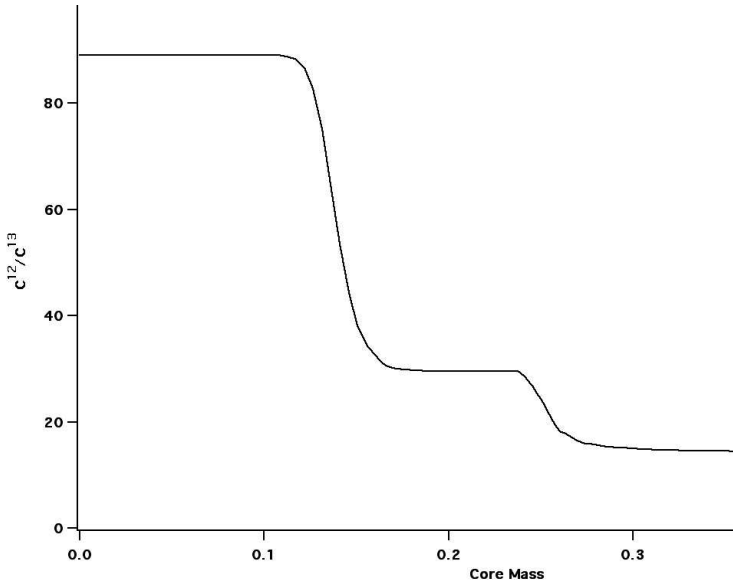

Figure 6 – The $^{12}C/^{13}C$ ratio versus core mass in a $1\,M_\odot$ model.

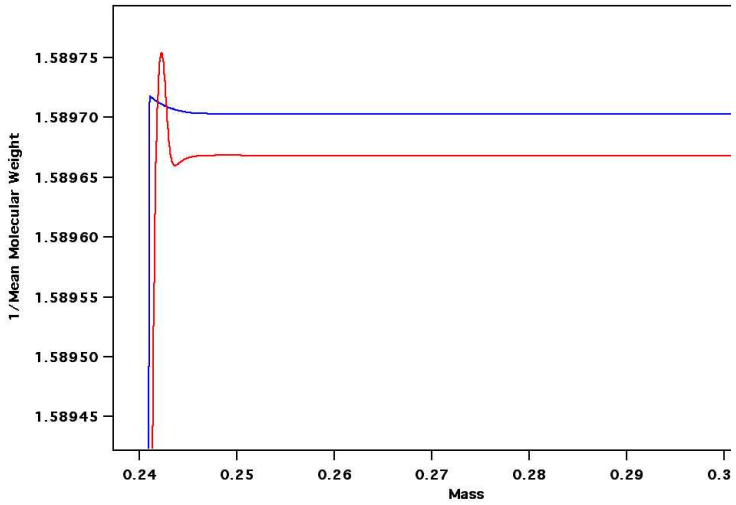

Figure 7 – Approximately 3 million years after the hydrogen burning shell approaches the homogeneous region, the $1/\mu$ profiles for a $1\,M_\odot$ model with no mixing (red) and a μ-boosted mixing model (blue).

To illustrate the effect on a star's evolution of this μ-boosted mixing, a $1\,M_\odot$ ($Z =$

0.02) model was evolved from a pre-main-sequence configuration to the helium core flash. The initial $^{12}C/^{13}C$ ratio was chosen to be 90, and as the model reached the giant branch ($M_{\rm core} \sim 0.2\,M_\odot$) the surface convection reduced the ratio to 29.5. When the new mixing mechanism began, the $^{12}C/^{13}C$ ratio declined rapidly to near 15 (Fig. 6). At this point, the reduced ^{3}He abundance slowed the mixing to the extent that between a core mass of 0.3 and $0.45\,M_\odot$ the ratio declined only to 14.3. Nearly 93% of the ^{3}He present when the mechanism started was destroyed.

When the μ-boosted mixing is active, the striking molecular weight inversion (red in Fig. 7) does not develop. Instead, a much more gradual profile is developed with a modest cusp in the region where the ^{3}He burning occurs.

6. Sensitivity of the $^{12}C/^{13}C$ ratio and ^{3}He destruction to $F_{\rm inv}$

To test the sensitivity of the ^{3}He destruction and the final $^{12}C/^{13}C$ ratio to the factor $F_{\rm inv}$, a series of runs were made on a $1\,M_\odot$ $Z = 0.02$ model. The value of $F_{\rm inv}$ was varied over a factor of 10,000 (from 0.01 of the standard value to 100 times the standard value). To test the sensitivity to mesh resolution, this test was done for a model with 300 zones and another with 750 zones.

Table 1 – Effects of varying $F_{\rm inv}$ and Number of Zones

	300 Zones		750 Zones	
Factor	$^{12}C/^{13}C$	^{3}He Destroyed	$^{12}C/^{13}C$	^{3}He Destroyed
0.01	18.9	59.0%	27.8	35.8%
0.03	14.0	75.8%	22.9	46.7%
0.10	12.2	87.3%	16.1	64.9%
0.30	12.3	91.3%	12.2	80.6%
1.00	13.4	92.6%	11.1	89.1%
3.00	15.7	92.4%	11.7	91.9%
10.0	16.1	92.8%	12.7	93.1%
100	16.5	93.9%	14.1	93.8%

Table 1 shows that factors 1/100th to 1/10th of the adopted standard value (representative of cloud rise rates less than 0.1 cm/s) are too slow and the ^{3}He burning is very incomplete. For rates near the standard value chosen, destruction is near 90%, and $^{12}C/^{13}C$ ratios are a minimum. Larger diffusion coefficients only modestly reduce the ^{3}He abundance and give a little less reduction in $^{12}C/^{13}C$. The table also shows a modest sensitivity to mesh resolution. In the absence of μ-boosted mixing, these models gave $^{12}C/^{13}C$ ratios of 29.5 and

29.1.

Next we examined a range of masses (for $Z = 0.02$, and 300 zones) comparing diffusion coefficients that differ by a factor of 100. For the higher diffusion coefficients, differing by a factor of 100, the ^{3}He destruction is almost identical except for the higher mass where less ^{3}He is produced in the first place. There are modest differences in ^{12}C/^{13}C ratios that at present should be considered as uncertainty in the modeling of the mechanism.

Table 2 – Effect of varying mass and $F_{\rm inv}$

		1×	1×	100×	100×
Mass	PreMix	Mixed	^{3}He Destroyed	Mixed	^{3}He Destroyed
0.80	36.9	15.9	96.4%	19.5	96.7%
0.85	34.0	15.3	95.7%	18.5	96.0%
0.90	32.2	14.5	94.8%	17.6	95.4%
1.00	29.5	13.4	92.6%	16.5	93.5%
1.25	25.6	13.0	85.7%	14.9	89.1%
1.50	23.6	13.7	74.9%	14.4	82.3%
2.00	22.3	17.0	45.1%	14.9	63.6%

Table 2 shows that the behavior seen in the $1\,M_\odot$ model holds over the range of interesting masses. Between 0.8 and $2.0\,M_\odot$, higher diffusion coefficients result in small changes in the ^{3}He destruction, and very modest differences in ^{12}C/^{13}C ratios. The differences in ^{12}C/^{13}C ratios caused by varying mesh and mixing coefficient (± 2 for Pop I models) should be considered uncertainty in the modeling of the mechanism (at present). When the ratio drops to near the equilibrium value of 3.5, as we will see in Pop II models, these factors have much less effect on the ^{12}C/^{13}C ratios.

7. ^{12}C/^{13}C and μ-Boosted Mixing

The following section examines the ^{12}C/^{13}C ratios, and the helium production a range of low mass stars with Pop I and Pop II metallicities. We use the standard diffusion coefficient developed above for the μ-boosted mixing. Consistent with Anders & Grevesse (1989), the initial ^{3}He mass fraction was taken to be 2×10^{-5}. While it is appropriate to use a higher value to account for the conversion of D to ^{3}He on the pre-main sequence, this difference is minor when compared to the main sequence production of low mass stars.

Table 3 shows the ^{12}C/^{13}C ratios for models ranging from 0.8 to $2.0\,M_\odot$, and for metallicities from solar to 1/50th solar. In the absence of an additional mixing process, the final

(tip of Giant Branch) value of the carbon isotope ratio depends on mass. As the mass rises from 0.8 to 2.0 $M_\odot$, the expected $^{12}C/^{13}C$ ratio drops from near 35 to near 20, with very little dependence on Z. This mass dependence is seen in the PreMix columns of table 3, showing the $^{12}C/^{13}C$ values before μ-boost mixing begins. Once the mixing begins, the $^{12}C/^{13}C$ ratio rapidly drops to a lower value, and the final range of ratios (Mixed) show a considerably reduced range. For solar metallicities, stars in this mass range all show $^{12}C/^{13}C \approx 14.5 \pm 1.5$. Similarly, for Z = 1/50th solar, $^{12}C/^{13}C \approx 4.0 \pm 0.5$. The 2.0 $M_\odot$ models are not included in these averages, as the μ-boosted mixing begins just prior to helium core flash in the Pop I model, and has not begun in the $Z = 0.0004$ model.

Table 3 – $^{12}C/^{13}C$ ratios

	X=0.70, Z=0.02		X=0.738, Z=0.001		X=0.74, Z=0.0004	
Mass	PreMix	Mixed	PreMix	Mixed	PreMix	Mixed
0.80	36.9	15.9	34.1	5.3	35.0	4.2
0.85	34.0	15.3	31.5	5.0	31.8	4.0
0.90	32.2	14.5	29.6	4.9	30.0	4.0
1.00	29.5	13.4	27.3	4.9	27.4	4.0
1.25	25.6	13.0	24.3	5.0	24.3	4.1
1.50	23.6	13.7	24.3	5.2	22.7	4.6
2.00	22.3	17.0	21.2	14.2	21.0	21.0

The result that post-mixing $^{12}C/^{13}C$ values converge for a broad range of masses is an interesting result, and is shown graphically in Fig. 8. Before μ-boosted mixing begins, the carbon isotope ratios show the usual mass dependent range, but not afterwards. To illustrate Z dependence in more detail, a star of mass 0.9 $M_\odot$ was evolved with various values of Z between solar and 1/200th solar (Fig. 9). The $^{12}C/^{13}C$ ratio is seen to vary smoothly from 14.8 to 3.5. Additionally there are big change in $^{14}N/^{15}N$, and small changes in O isotope ratios (mostly due to ^{18}O and ^{17}O). Table 4 provides the same information in tabular form.

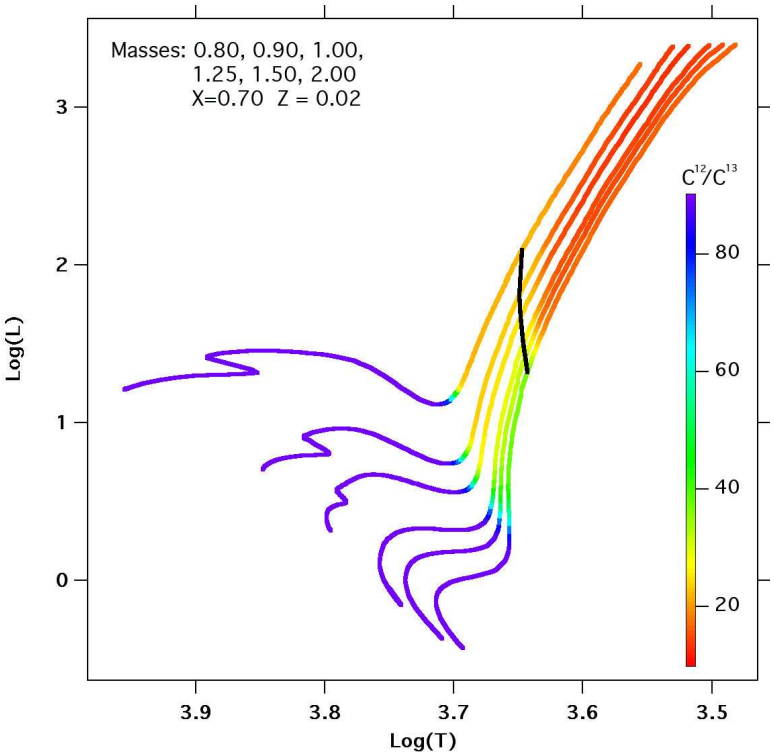

Figure 8 – $^{12}C/^{13}C$ ratio for various masses using the standard $F_{\rm inv}$. The black line shows where μ-boosted mixing begins.

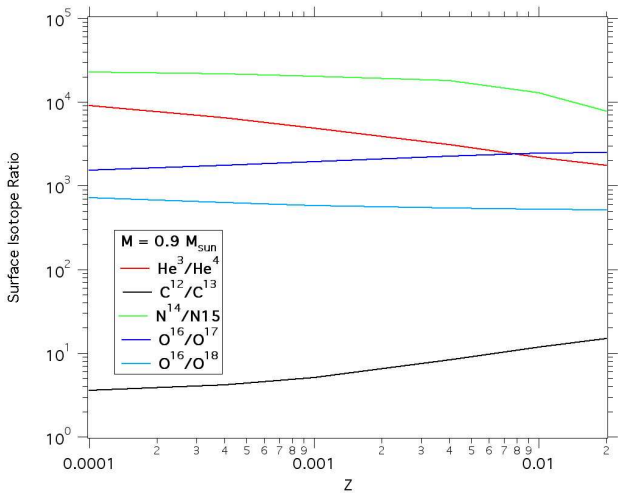

Figure 9 – Post-mixing, surface isotope ratios in a $0.9\,M_\odot$ model with a large range of initial abundances.

Table 4 – Surface Isotope Ratios at top of the Giant Branch

Z	^{3}He/^{4}He	^{12}C/^{13}C	^{14}N/^{15}N	^{16}O/^{17}O	^{16}O/^{18}O
0.02	1.8×10^{3}	14.5	0.8×10^{4}	2.5×10^{3}	513.
0.01	2.3×10^{3}	11.3	1.4×10^{4}	2.4×10^{3}	521.
0.004	3.2×10^{3}	8.0	1.8×10^{4}	2.3×10^{3}	537.
0.001	5.2×10^{3}	4.9	2.1×10^{4}	1.9×10^{3}	584.
0.0004	6.8×10^{3}	4.0	2.2×10^{4}	1.7×10^{3}	640.
0.0001	9.1×10^{3}	3.5	2.3×10^{4}	1.5×10^{3}	752.

In the low-mass stars of interest here, the PP chain dominates evolution on the main sequence, but the hydrogen-burning shell on the giant branch operates on the CNO cycle. With fewer CNO nuclei, the shell must burn at a somewhat higher temperature for the same energy production rate. Additionally, the penetration of the surface convection region is not as deep at low Z, and the inversion is not initiated until the core grows to a larger mass. These effects combine to result in a higher temperature in the place where the molecular weight inversion develops. As Z decreases from 0.02 to 0.0001, the core mass at which the inversion occurs increases (from 0.233 to 0.358 for models of mass $0.9\,M_{\odot}$). The luminosity, $\log L$, at the start of mixing increases from 1.4 to 2.4, and the temperature at the base of the mixing increases from 16.5 million K to 24.0 million. As a result, the mixing begins at a metallicity-dependent temperature, and the ^{12}C/^{13}C ratio achieves different enhancement before the reduced ^{3}He abundance slows the process (Fig. 10).

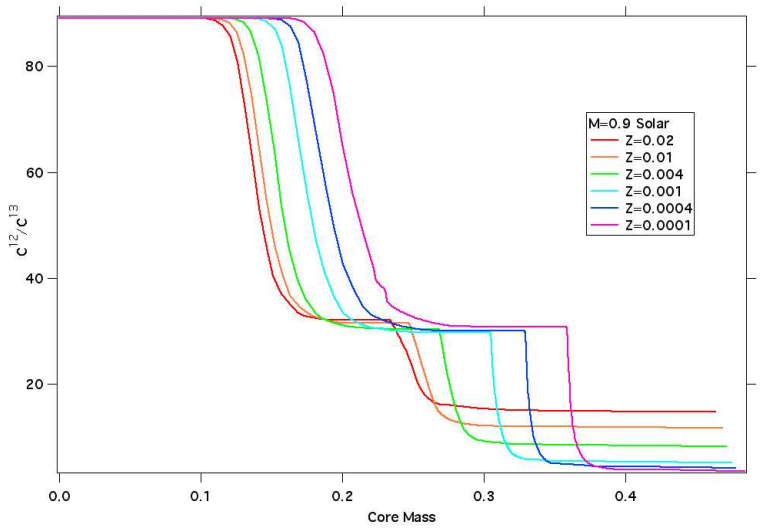

Figure 10 – The ^{12}C/^{13}C ratio verses core mass for a range of metallicities.

As a final note, these models were all run with a mixing length that was 1.8 pressure scale heights (to fit the solar radius). Changing the mixing length ± 0.2 resulted in changes in the $^{12}C/^{13}C$ ratio that were < 0.4.

8. The Metallicity Effect and Observations

Gilroy & Brown (1991) measured the carbon isotope ratios in the stars of M67 (near $1.2\,M_\odot$). They report that 'the subgiants seem to have undergone little or no mixing', and that the lower giant branch stars exhibit 'normal first dredge-up mixing ratios'. However they find 8 upper giant branch and clump giants with $^{12}C/^{13}C$ ratios between 11 and 15. This is in excellent agreement with the value near 13.5 that results from μ-boosted mixing (Table 3). At the lower metal enrichments, Pavlenko et al. (2003) observed giants in the globular clusters M3, M5, and M13 ([M/H] $= -1.3, -1.4$, and -1.6 or $Z \leq 0.001$), finding $^{12}C/^{13}C$ between 3 and 5. Again this is in excellent accord with our models (Table 3). They also observed M71 ([M/H] $= -0.71$ or $Z \approx 0.004$) finding less processing. Here the $^{12}C/^{13}C$ ratios show values near 7 (5 to 9). The $0.9\,M_\odot$ model that we used to illustrate the metallicity effect gives an expectation for $^{12}C/^{13}C$ ratios near 8.

9. ^{3}He and μ-Boosted Mixing

As stated earlier, in the calculations done here the initial mass fraction of ^{3}He was taken to be 2×10^{-5}. In Table 5, a $0.9\,M_\odot$ model is evaluated for a range of metallicities to find the peak enhancement in the mass of ^{3}He, M(^{3}He,peak)/M(^{3}He,init). For solar composition, the enhancement reaches a factor of 61. With shorter main sequence lifetimes, Pop II models of this mass reach only about 38. Increasing the main sequence value of ^{3}He by an order of magnitude, to 2×10^{-4}, by assuming all of the deuterium is burned to ^{3}He on the pre-main sequence makes surprisingly little difference. For Pop I abundances, starting with an enhanced initial ^{3}He abundance associated with converting ^{2}H to ^{3}He results in a peak enhancement of 64 times the ISM ^{3}He used to form the star (2×10^{-5}) instead of 61. For an extreme Pop II metallicity, the peak enhancement is 41 instead of 38.

Table 5 – ^{3}He production in a $0.9\,M_\odot$ model.

Z	0.02	0.01	0.004	0.001	0.0004	0.0001
Peak	61.1	56.5	48.7	40.0	38.7	38.1
Final	3.1	2.3	1.6	1.0	0.7	0.5
Change	94.8%	95.8%	96.7%	97.6%	98.1%	98.6%

These very large peak enhancements were problematic in reconciling stellar nucleosynthesis and Big Bang nucleosynthesis with observed abundances. With μ-boosted mixing the final enhancement for Pop I abundances is reduced to 3.1 (3.4 when ^{2}H conversion is included), and for Pop II models the final value is 0.52 (0.53 with ^{2}H conversion).

Table 6 shows the same behavior for stars in the mass range of 0.8 to 2 $M_\odot$. Table 6 shows the ratio of the peak Pre-mix mass of ^{3}He to the original mass of ^{3}He in the star, as well as the post-mixing ratio

Table 6 – ^{3}He/^{3}He (original)

	X=0.70	Z=0.02	X=0.738	Z=0.001	X=0.74	Z=0.0004
M	Peak	Mixed	Peak	Mixed	Peak	Mixed
0.80	76.6	2.7	54.7	0.86	53.0	0.62
0.85	68.2	2.9	46.5	0.90	45.1	0.66
0.90	61.1	3.1	40.0	0.95	38.7	0.73
1.00	49.7	3.7	32.9	1.12	30.0	0.83
1.25	31.7	4.5	21.8	1.60	19.9	1.21
1.50	21.8	5.5	15.7	2.08	14.4	1.91
2.00	12.8	7.0	9.5	6.70	8.7	8.39

As found in earlier papers, the greatest potential ^{3}He enhancement occurs for stars of 1 $M_\odot$ and below. In these models, it is the large ^{3}He enhancement that enables the μ-boosted mixing to destroy 90 to 95% of the potential ^{3}He contribution to the interstellar medium. As a final note, below 2 $M_\odot$, the μ-boosted mixing operates to (near) completion only for the Pop I model. In the $Z = 0.001$ calculation, the mechanism begins just prior to the helium flash and is incomplete. In the $Z = 0.0004$ model, the helium core flash precedes any significant μ-boosted mixing.

10. ^{16}O and ^{23}Na with μ-Boosted Mixing

Some observational evidence has suggested that ^{16}O and ^{23}Na may change on the upper giant branch. In the 1.5 $M_\odot$ models run with $Z = 0.02$ and 0.0001, there was substantial ^{23}Na enhancement: $\delta(^{23}\mathrm{Na}) \approx 19\%$ and 68%. However, this was just the usual enhancement expected from main sequence processing followed by giant branch mixing, and is not significantly effected by μ-boosted mixing. When we examined the 0.9 $M_\odot$ model the greatest change was seen for the extreme Pop II abundance (1/200th solar), where the ^{23}Na abundance climbs by 3%. Only about half of this change is due to μ-boosted mixing. The ^{16}O depletion is a trivial 0.25% (Fig. 11).

In low mass, low metallicity stars, the μ-boosted mixing brings the effective bottom of the convection zone to a point where ^{16}O and ^{23}Na are beginning to change. Because of this the change in these isotopes is dependant on the location that the mixing model finds for the base of the μ-boosted mixing, where the mixing and burning of ^{3}He are in balance. The mixing model developed here does not appear sufficient to explain an observable ^{16}O depletion or ^{23}Na enhancement, but this result warrants additional investigation. Because of the temperature sensitivity, a modest amount of undershoot, or turbulent mixing, could change this result.

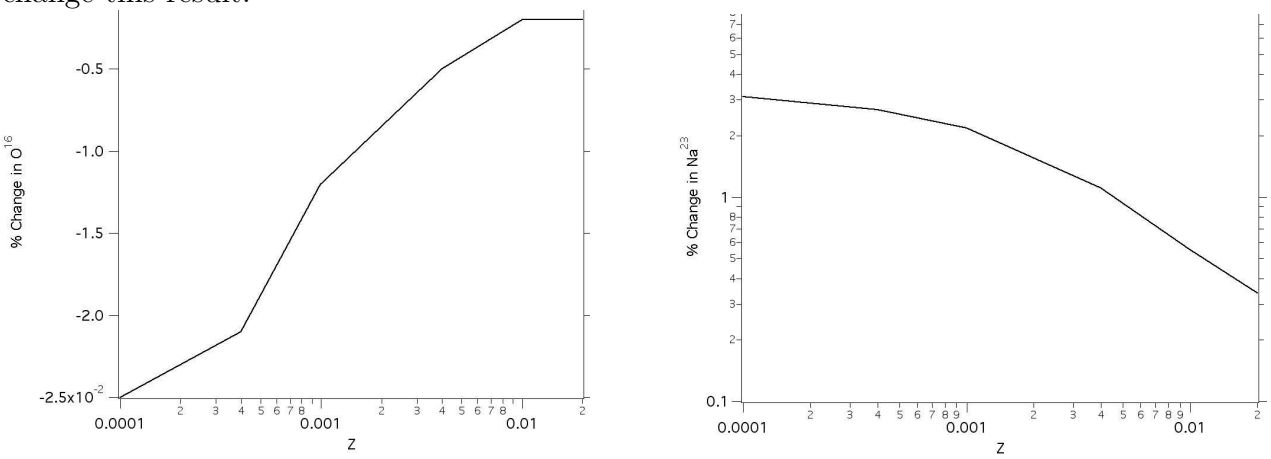

Figure 11 – Change in the surface abundance of ^{16}O and ^{23}Na in a $0.9\,M_{\odot}$ model evolved with various metallicities.

11. Mass Loss after the mixing does not matter

As noted in the introduction, the blue horizontal branches of globular clusters indicate that a substantial fraction of the envelope is lost prior to the helium core flash. This was the origin of the excess ^{3}He production by these stars. With this new mixing mechanism, once the inversion occurs, the ^{3}He abundance drops rapidly. As the mixing depends on the square of the ^{3}He abundance, the process slows dramatically when 90% of this isotope has been consumed. Mass loss after this rapid drop does not cause contamination problems with excess ^{3}He, and leads to little change in the surface abundances or yields. To illustrate this, a $0.8\,M_{\odot}$ $Z = 0.0001$ model was run with no mass loss, and then again with $0.2\,M_{\odot}$ of mass loss near the tip off the giant branch (and after the μ-boosted mixing). The surface abundances show little change from the mass loss.

In the absence of μ-boosted mixing, the mass losing model ejects 52 times as much ^{3}He into the ISM as it took when it formed. This was the basis of the problem of reconciling Big

Bang nucleosynthesis with yields from stellar evolution. With μ-boosted mixing, the mass loss ejects 1/3rd of the ^{3}He into the ISM as it took when the star formed, and retains only 1/7th of the intake to be further processed or ejected.

Table 7 – Enhancements with and without Mass Loss

Isotope Ratios	No Loss	Loss
^{3}He/^{4}He	9065.5	9466.7
^{12}C/^{13}C	3.5	3.5
^{14}N/^{15}N	22564.1	22330.
^{16}O/^{17}O	1913.4	1920.8
^{16}O/^{18}O	702.6	677.8
$\delta(^{16}$O)	-0.01%	-0.01%
$\delta(^{23}$Na)	1.2%	1.3%

12. Conclusions

Our first conclusion is that μ-boosted mixing is a significant and inevitable process in low-mass stars ascending the giant branch for the first time. Once it begins, the timescale is short, and it maintains a homogeneous composition down to base temperatures in the region of 16 to 25 million K, allowing nuclear processing. The result is an observable change in the expected abundances of ^{3}He and the CNO isotopes.

This mixing mechanism is driven by the destruction of ^{3}He, and is self-limiting. The lowest mass stars ($< 1.25\,M_\odot$), that were expected to produce a problematic excess of ^{3}He, quickly destroy 90 to 95% of that isotope. As a result, the ^{3}He returned to the ISM is within the limits posed by Hata et al (1995). This mixing also modifies the ^{12}C/^{13}C ratios. Instead of showing a significant mass dependence in that ratio, we find a metallicity dependence instead. Shortly after this mixing begins, Pop I stars between 0.8 and 2.0 $M_\odot$ should all drop to a value near 14.5. Extreme pop II stars in this mass range should show ratios near 4. Likewise the nitrogen and oxygen isotope ratios are substantially affected (Figure 12).

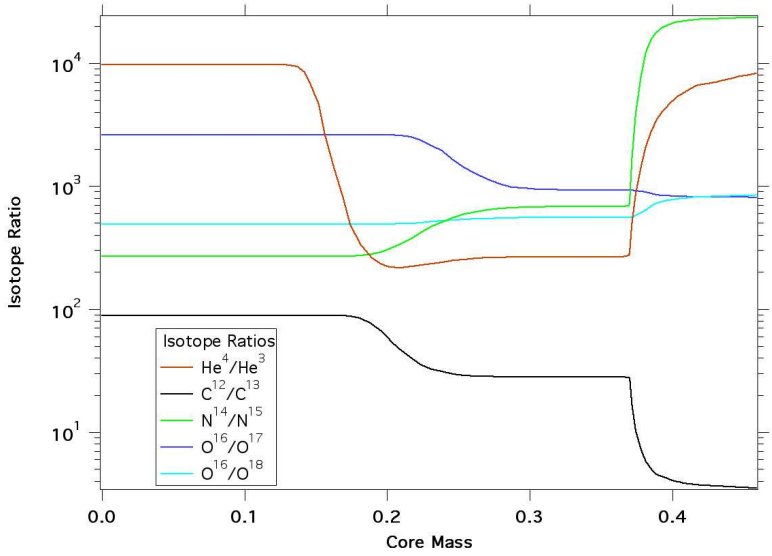

Figure 12: CNO isotope ratios in a 1 $M_{\odot}$ ($Z = 0.0001$) model are plotted against core mass.

As a first effort to develop a 1D model for this mixing process, we have tried to validate it with reference to the original 3D modeling, and basic physical arguments. At the moment, variations due to mesh resolution and mixing speed suggest an uncertainty of ± 2 for Pop I values of the $^{12}C/^{13}C$ ratio (much less for Pop II). The fractional destruction of ^{3}He seems less sensitive to such choices. We have also held the initial isotope ratios fixed ($^{12}C/^{13}C = 90$, $^{14}N/^{15}N = 270$, $^{16}O/^{17}O = 2625$, and $^{16}O/^{18}O = 490$), and different values must be run to study chemical evolution.

Finally, this process does not appear to have significant impact on the ^{16}O depletion or ^{23}Na enhancement, but with the temperature sensitivity of these rates, it comes close. Any overshoot in the mixing at the bottom of the region will be important. Also, the thickness of the stable region that surrounds the hydrogen burning shell is reduced from over a solar radius to a few hundredths of a solar radius. This may enable other mechanisms (rotation, magnetic fields, ...) to create variation in the observed abundances. Alternatively, the homogeneity seen in clusters like M67 (Gilroy & Brown 1991) might be used to limit models for rotational mixing.

13. Acknowledgments

This study has been carried out under the auspices of the U.S. Department of Energy, National Nuclear Security Administration, by the University of California, Lawrence Livermore National Laboratory, under contract No. W-7405-Eng-48. JCL was partially supported

by the Australian Research Council. We are indebted to R. Palasek for assistance with the code..

REFERENCES

Anders, E. & Grevesse, N., 1989, Geochim. Cosmochim. Acta, vol. 53, 197

Caughlan, G. R. & Fowler, W. A., 1988, At. Data Nucl. Data Tables, 40, 284

Chaname, J., Pinsonneault, M. & Terndrup, D., 2005, ApJ, 631, 540

Charbonnel, C., 1995, ApJ, 453, L41

Dalhed, H. E., Wilson, J. R. & Mayle, R. W., 1999, Nuc. Phys. B – Proceedings Supplements, 77, Issues 1 – 3, p429

Day, B. A., Lambert, D. L. & Sneden, C., 1974, ApJ, 185, 213

Dearborn, D. S. P., 1992, Phys. Rep., 210, 367

Dearborn, D. S. P., Eggleton, P. P. & Lattanzio, J. C., 2006, ApJ, 639, 405 (Paper I)

Dearborn, D. S. P., Eggleton, P. P. & Schramm, D. N., 1976, ApJ, 203, 455

Dearborn, D. S. P., Lambert, D. L. & Tomkin, J., 1975, ApJ, 200, 675

Dearborn, D. S. P., Schramm, D. N. & Steigman G., 1986, ApJ, 302, 35

Dearborn, D. S. P., Steigman, G. & Tosi, M., 1996, ApJ, 465, 887

Eggleton, P. P., Dearborn, D. S. P. & Lattanzio, J. C., 2006a, Science, 314, 1580 (Paper II)

Eggleton, P. P., Dearborn, D. S. P. & Lattanzio, J. C., 2006b, in *Convection in Astrophysics*, IAU Symp. 239, eds Kupka, F. & Roxburgh, I. W., in press (Paper III)

Gilroy, K. K. 1989, ApJ, 347, 835

Gilroy, K. K. & Brown, J. A., 1991, ApJ, 371, 578

Harris, M. & Lambert, D. L., 1984a, ApJ, 281, 739

Harris, M. & Lambert, D. L., 1984b, ApJ, 284, 223

Hata, N., Scherrer, R. J., Steigman, G., Thomas, D., Walker, T. P., Bludman, S. & Langacker, P., 1995, Phys. Rev. Lett. 75, 3977

Hogan, C. J., 1995, ApJ, 441, L17

Hubbard, E. & Dearborn, D. S. P., 1980, Ap. J., 239, 248

Lambert, D. L. & Dearborn, D. S. P., 1972, Memoires Société Royale de Sciences de Liège, 6 series, tome III, p. 147

Palacios, A., Charbonnel, C., Talon, S. & Seiss, L., 2006, A&A (submitted).

Pavlenko, Y. V., Jones, H. R. A. & Longmore, A. J., 2003, MN, 345, 311

Steigman, G., Dearborn, D. S. P. & Schramm, D. N., 1986, in *Nucleosynthesis and its implications on nuclear and particle physics*, eds Audouze, J. & Mathieu, N. NATO ASI Series, Volume C163, p37.

Tomkin, J. & Lambert, D. L., 1978, ApJ, 223, 937

Tomkin, J., Lambert, D. L. & Luck, R. E., 1975, ApJ, 199, 436

Tomkin, J., Luck, R. E. & Lambert, D. L., 1976, ApJ, 210, 694

Tout, C. A. & Smith, G. H., 1992, MN, 256, 449

Wasserburg, G. J., Boothroyd, A. & Sackmann, I.-J., 1995, ApJ, 447, L37

Weiss, A. & Charbonnel, C., 2004, Mem. S.A.It. 75, 347

Wilson, J. R. & Mayle, R. W., 1988, Phys. Rep., 163, Nos 1 – 3, 63